

Enhancement of Convective Heat Transfer in a Parabolic Trough Collector Using Vibrations—an Introductory Numerical Analysis

Krzysztof Grzywnowicz^{1✉}, Łukasz Bartela¹, Leszek Remiorz², and Bartosz Stanek³

¹Silesian University of Technology
✉krzysztof.grzywnowicz@polsl.pl

Abstract

Energy generation systems based on renewable energy sources (RES) are rapidly gaining ground in the global power and heat market. Most of these systems are well-suited to distributed energy solutions, including distributed heat production. Individual users and local low-power plants can use solar thermal devices for the purpose of providing domestic hot water, heating and cooling. Nevertheless, the variability of solar irradiance can make it difficult to harvest energy efficiently all year round. Therefore, from the point of view of improving the overall, year-averaged operational parameters of a solar thermal device it is paramount to maximize the heat acquired from it at times of high radiation flux. This paper discusses computational research on enhancing convective heat transfer in the absorber of a parabolic trough collector (PTC), through inducing vibrations of an immersed flat plate. The investigation identifies the influence of different amplitudes and frequencies of oscillatory motion on the absorber's parameters, compares them with the construction of a classical absorber and considers flow turbulence. The results indicate there is only a limited application of vibrations to enhance operational parameters of solar thermal absorbers, with the best results obtained for thermal fluid flows of below 0.1 dms.

Keywords: Concentrated solar power, Parabolic trough collector, Heat transfer enhancement, Convection intensification

1 Introduction

Fossil fuels are the primary energy source for the energy sector worldwide. Nevertheless, finite resources and rising climate concerns have promoted the introduction of power technologies based on renewable energy sources (RES) [1]. High instability, caused by seasonal and short-term variation of energy availability, meant that RES-based technologies were initially adapted to the distributed energy sector [2]. Sunlight is prominent among the primary energy sources harnessed for distributed systems and lies at the core of this paper [1]. Solar technologies are

used to induce electric current in photovoltaic (PV) cells and to generate useful energy as heat in thermal collectors [1]. Furthermore, PV-thermal hybrid units, producing both, are utilized as well [1]. Solar thermal units have a significant share of the solar energy market, caused primarily by their typically higher efficiency levels compared to solar-to-current systems [1, 3, 4, 5]. Fluctuations in energy accessibility, caused by fast-changing weather conditions and local geography, has encouraged research into various technologies to enhance energy output from solar units. Foremost among these is the concentration of direct solar radiation to light exclusively the absorber while reducing radiation dissipation and other losses [3, 6].

There has been a recent uptick in the intensity of research into sun radiation concentrators, due to their high application potential in PV [7], hybrid [8] and solely thermal units [9, 10]. Most investigations have focused on geometry and materials, modelling of the concentrators' optical properties, as well as design and optimization of complex systems, utilizing absorbed solar energy.

One strong focus has been on optical analysis of the geometry of parabolic trough collectors (PTC). PTCs could be manufactured at low cost and are easy to implement [11, 12, 13]. Current research in the field of PTC concerns advanced measuring devices [11] for accurate determination of optical properties of reflective coatings of mirrors, as well as fundamentals of their optimization [12, 14]. Other geometries of concentrated-energy thermal units are also attracting interest. Experimental research on parabolic satellite dishes (PSD), primarily in comparison with other available geometries, has been performed recently [15], as has deep investigation of conical solar concentrators including installation design strategy [16]. The results of other recent research show [17, 18, 19] that aplanat geometry concentrators seem to be comparably more advantageous in a number of applications. In addition to research con-

cerning classical geometry, studies have also sought to develop two-stage concentrators [9] and spectrum-splitting systems [20, 21], which might give advantages to next generation units. Alternatively, optimization of known solutions [12, 13, 22] might bridge the gap between existing state-of-the-art devices and technologies that are currently under development in laboratories.

There are major challenges to be overcome with solar irradiance concentrators. These include the risk of PV cells overheating [23] and local evaporation or thermal degradation of the heat carrier in thermal units [24, 25]. One fundamental disadvantage, following evaporation or degradation of the working fluid, even considering only a thin film located at the interface between the fluid and irradiated walls, might be a major decrease in convective heat transfer parameters. Since convection between the internal wall of the absorber and circulating medium is a fundamental form of heat transfer, any drop in its parameters brings with it a risk of damage to the device and of sudden change in the physical properties of the circulating fluid [6, 24]. Therefore, it is vital to enhance convection in solar thermal absorbers, especially for installations using concentrated radiation.

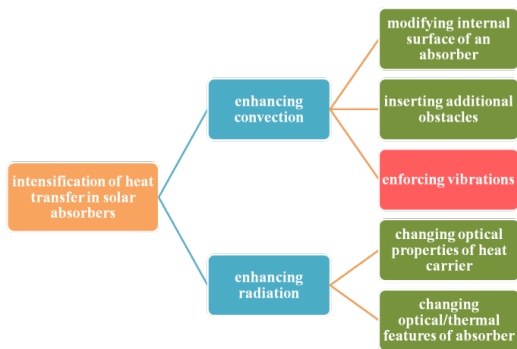


Figure 1: Overview of methods to intensify heat transfer in solar thermal units

Discussion of a number of studies on different techniques of intensification is given in: [26, 27, 28, 29, 30, 31, 32, 33]. Research presented in these papers includes the use of nanoparticles of carbon [26] or copper compounds [33, 27] as additives to the new generation of thermal fluids, to enhance conduction through the fluid and absorbance. The use of nanofluids, in essence classical high temperature fluids with added nanoparticles, might lead to a breakthrough in the field of solar thermal systems [28, 29]. However, widespread introduction of such fluids requires long-term research into their impact on the estimated service life of the power generating installation. Thus, more research is needed that focuses

on increasing the operational parameters of state-of-the-art designs. Current investigations concern primarily a variety of geometries of twisted or coil-like turbulizing elements [30] along with strongly aligned ribs [31] and wedge-shaped vertices that produce elements [32] which are inserted into the absorber’s interior.

Despite the profound research performed in this field, there has been little focus on the application of vibrations as a method to intensify heat transfer. Enhanced convection might be expected to result from turbulizing the flow of the circulating thermal fluid and local change in advection parameters. As the strongly beneficial influence of vibrations on heat transfer in practical utilities has been already proven and discussed in [34, 35, 36, 37], this approach might bring benefits to solar thermal devices too.

This paper focuses on numerical analysis of the effect of application of an immersed vibrating plate, which acts as a source of vertices to intensify convective heat transfer in the working fluid of a PTC absorber. Additional reference cases in the form of a classical construction with no heat transfer enhancement and an absorber with static turbulizing element inserted into the internal volume of the absorber, were simulated as well, for the purpose of comparing the investigated method and its macroscopic thermal effects with the state-of-the-art systems. The simulations utilized a 3D model, prepared and computationally investigated using commercially available numerical software.

2 Computational Model

The numerical model investigated the geometry of a concentrated solar irradiance receiver in the form of a cylindrical absorber, made of structural steel [38]. The geometry of the absorber is presented in Fig. 2. Two geometries, corresponding to simulated heat transfer enhanced devices, including immersed turbulizing device and vibrating plate, are shown in Fig. 3 and Fig. 4, respectively.

To simplify the geometry and reduce mesh volume, the CFD modelling excluded the parabolic trough, assumed as the concentrating element of the PTC unit [38]. APEX optical analysis software was used to perform computational ray tracing and numerical determination of irradiance in order to estimate the boundary conditions on the absorber’s external surface. The computations included preparation of three-dimensional geometry of a parabolic concentrator to be used in a standard PTC installation.

The geometry consisted of a tubular absorber of geometry, as per Fig. 1, and a parabolic shaped mirror.

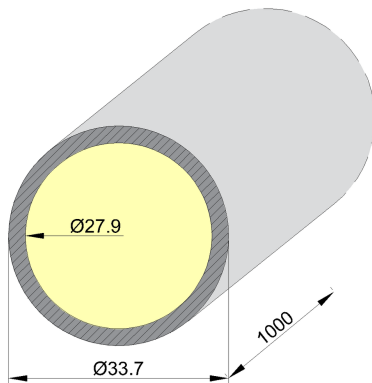


Figure 2: Geometry of the modelled absorber

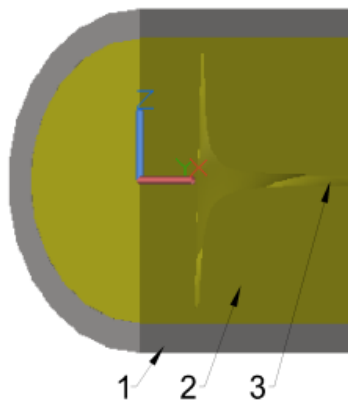


Figure 3: Geometry of the absorber with immersed spiral turbulizing device: 1 - absorber, 2 - thermal fluid, 3 - walls of the spiral device

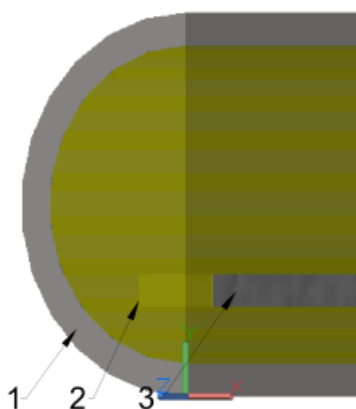


Figure 4: Geometry of the absorber with vibrating plate: 1 - absorber, 2 - thermal fluid, 3 - immersed plate

The absorber was located directly in the concentrator’s focal point. Drawing on the available library of properties of coatings in the APEX environment, coatings were selected for both elements. Protected silver coating was selected for the parabolic mirror. This coating enjoys the highest reflectivity stability as a function of wavelength. Absorber surface absorptency was assumed at 80%. Optical modelling took into account the imperfections of the mirror surface, but excluded contamination. Thus, the mirror surface was assumed to be perfectly clean and to retain its optical parameters. The total loss resulting from the optical assumptions was 29.14%. A virtual element reflecting solar-like radiation was used to model the light source. Only solar direct irradiance was used for the calculation. Due to the negligible impact on the results, indirect radiation was not included. Furthermore, it is not possible to determine the value or angle of incidence of diffuse radiation, whose high variability derives from being reflected from intermediate elements that do not form part of the PTC infrastructure.

The selected optical-engineering software performs ray-tracing of radiation emitted from a given surface, determining its path and reflection from individual elements. APEX uses the Monte Carlo method. The software determined radiation distribution on the target surface and the value of energy supplied to the given element. The optical model of the parabolic trough with part of the cylindrical absorber, presenting the ray-tracing results, is shown in Fig. 5.

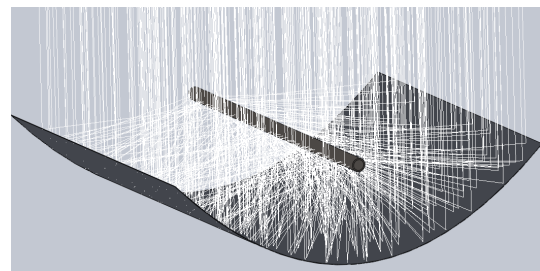


Figure 5: The optical model of the PTC

The detailed optical analysis, performed in a dedicated environment, identified the key boundary conditions of the system. These conditions, including the inclination angle of virtual surfaces, dividing the absorber into parts lit by the concentrated radiation and by the reference direct normal irradiance (DNI), as well as the derived mean radiative heat flux, were then introduced to the ANSYS software to perform the CFD analysis.

Other boundary conditions of the model, including primarily inlet and outlet parameters, were identified on the basis of an holistic analysis of the general dataset

Table 1: Key boundary conditions.

Parameter	Value
Total area of absorber, irradiated by concentrated light, mm^2	48.510 ³
Emissivity of the absorber walls, -	8.510 ⁻¹
Irradiance transferred to the directly irradiated surface, W/m^2	1000.0
Radiative heat flux on the absorber surface, W	708.6
Mean pressure of the circulating fluid, bar	1.3
Initial temperature of the circulating fluid, °C	30.0

for PTCs [6]. The properties of the circulating fluid (Therminol VP-1®), phenyl-based high temperature thermal oil) were taken from the literature [39]. The geometrical and environmental boundary conditions set during the simulation are listed in Table 1.

Apart from the boundary conditions, set at the external surfaces of the control volume of the numerical model, consideration was given to the model equations. The main issue focused on selection and implementation of highly-reliable, stable and accurate models of turbulences, which are expected to arise in the boundary layer due to implementing the static turbulizing devices and vibrating elements. The main challenge when considering possible models is the partially unknown and variable nature of turbulent vertices, which occur in the fluid domain due to the presence of static or vibrating elements. Thus, a complete model had to be implemented that covered a wide range of turbulence, in this case the Reynolds stress model, as indicated by Eq. 1 in the SSG variant [38, 40]. In order to define pressure and velocity distribution at the entrance and outlet of the absorber, average turbulence of 5% was applied to these boundaries.

Consideration was given to selection of the radiation model – since radiation is the only way of propagating energy outside the absorber’s external surface and might contribute to heat transfer at the absorber-fluid internal interface, high modelling accuracy was required.

$$\begin{aligned} \frac{\partial}{\partial t} (\overline{\rho u'_i u'_j}) + \frac{\partial}{\partial x_k} (\overline{\rho u_k u'_i u'_j}) = \\ - \frac{\partial}{\partial x_k} \left[\overline{\rho u'_i u'_j u'_k} + p' (\delta_{kj} u'_i + \delta_{ik} u'_j) \right] \\ + \frac{\partial}{\partial x_k} \left[\mu \frac{\partial}{\partial x_k} (\overline{u'_i u'_j}) \right] \end{aligned}$$

$$\begin{aligned} - \rho \left(\overline{u'_i u'_k} \frac{\partial u_j}{\partial x_k} + \overline{u'_j u'_k} \frac{\partial u_i}{\partial x_k} \right) \\ + p' \left(\frac{\partial u'_i}{\partial x_j} + \frac{\partial u'_j}{\partial x_i} \right) - 2\mu \frac{\partial u'_i}{\partial x_k} \frac{\partial u'_j}{\partial x_k} \\ - 2\rho \Omega_k \left(\overline{u'_j u'_m} \varepsilon_{ikm} + \overline{u'_i u'_m} \varepsilon_{jkm} \right) \quad (1) \end{aligned}$$

where: $R_{ij}, R_{ik}, R_{jk}, R_{ijk}$ – averaged vector products of Reynolds stresses in respective directions, t – time, u'_i, u'_j, u'_k – individual Reynolds stresses, ρ – density of the fluid, x_i, x_j, x_k – boundary layer coordinates, p – pressure, μ – dynamic viscosity of fluid, $\varepsilon_{ikm}, \varepsilon_{jkm}$ – dissipation terms, ν – kinematic viscosity of fluid.

Thus, consideration was given to the Monte Carlo and Discrete Transfer models, available in ANSYS CFX software. The fundamental assumption included in the Monte Carlo model is the proportionality of radiation intensity to the differential angular flux of incident photons [41]. Regarding the radiation field as a virtual “photon gas”, the absorption phenomenon is considered as the probability per unit length that a photon is absorbed at a given wavelength [41]. Therefore, the calculated mean radiation intensity (given by Eq. 2 [42]) is indirectly calculated on the basis of probability theory [42, 41].

In order to increase the accuracy of results and include fundamental radiation physics within the domain of the circulating heat carrier, the spectral model of gray body was assumed. Finally, convective heat transfer between the circulating fluid and the absorber was modelled as well. Convective heat transfer was assumed to be determined through recalculation of the energy balance, solved computationally by selected CFD software.

$$F_\nu = \int \frac{dE_\nu}{\cos\theta dA dt d\nu} \quad (2)$$

where: F_ν – energy flux, dE_ν – radiant energy of photon, θ – angle of inclination of the photon pathway to the normal of the incident surface, A – area of the incident surface, t – time, ν – frequency of the electromagnetic wave.

3 Results and Discussion

The results of the numerical simulations are presented in the form of temperature distributions at the absorber outlet, obtained for the respective cases, in-

licated on Fig.6 through Fig.11. The contours presented in Fig. 6 - 7 and Fig. 8 - 9 show the distributions obtained for the reference cases with no heat transfer intensification and with the immersed, spiral-shaped turbulizing device, respectively. The contours indicated in Fig. 10 - 11 plot the temperature distributions obtained for the modelled case of a flat plate, vibrating at a frequency of 50Hz and with an amplitude of 0.25mm.

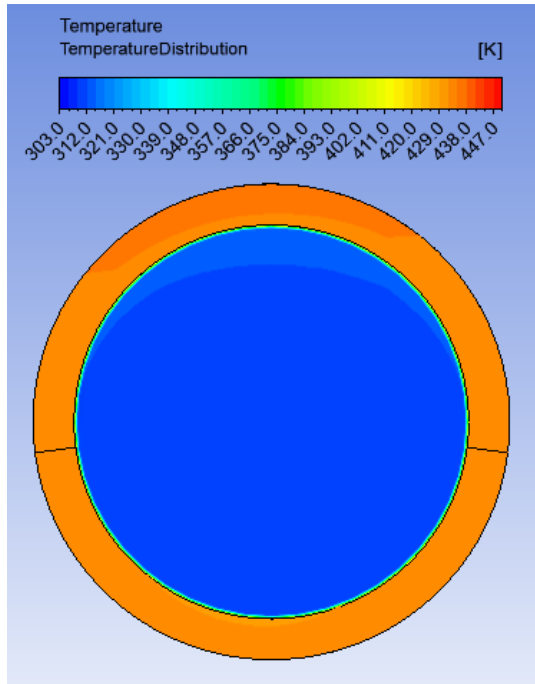


Figure 6: Temperature distribution at the absorber outlet for the reference state and fluid flow of $Q=0.05\text{dm}^3/\text{s}$

Results concerning the temperature distribution indicate key differences in local temperatures of the reference absorber, which does not apply any heat transfer enhancement technique. For thermal fluid flow five times greater than its minimum value, the average temperature of the absorber solid at the outlet dropped by roughly 70°C . Nevertheless, for both cases of modified absorbers, no major change was observed, although minor differences did appear. Considering the vibrating plate, a rise in circulating fluid flow was followed by a significant change in temperature distribution at the outlet in the domain of the fluid. However, as can be seen on Fig. 10, the major thermal effect of vibrations is on the lower wall of the absorber, the wall receiving concentrated radiation. This observation proves the potential of the technique to reduce the temperature of the wall, which experiences the highest temperatures of any element in the system.

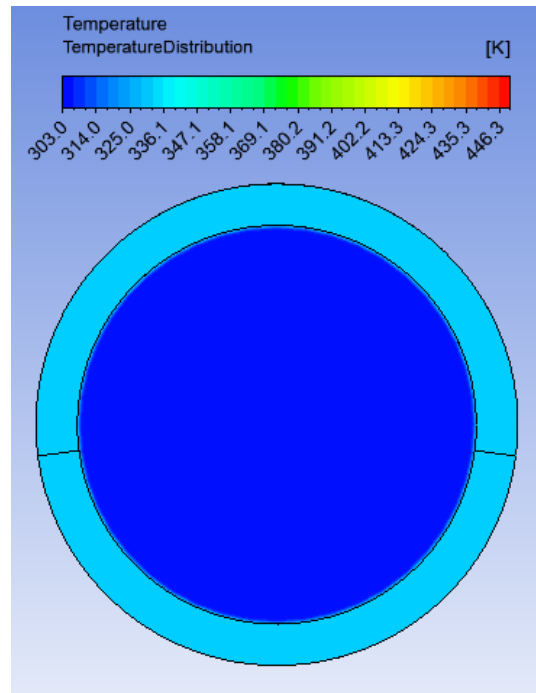


Figure 7: Temperature distribution at the absorber outlet for the reference state and fluid flow of $Q=0.25\text{dm}^3/\text{s}$

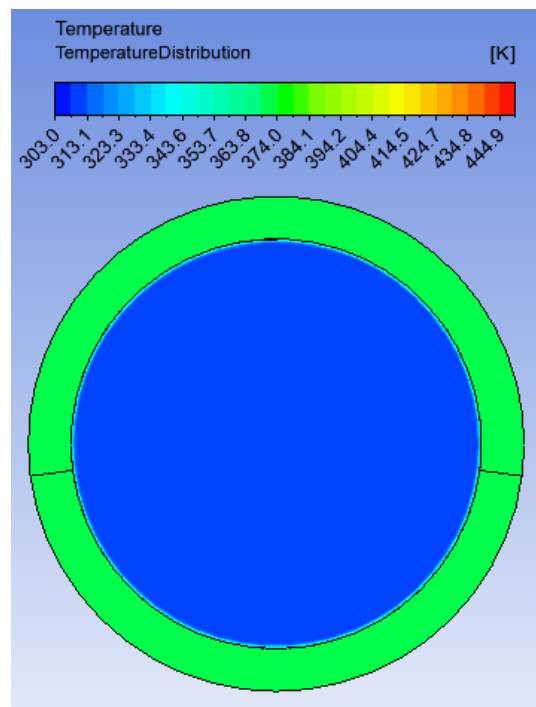


Figure 8: Temperature distribution at the absorber outlet for the reference immersed turbulizing device and fluid flow of $Q=0.05\text{dm}^3/\text{s}$

Curves showing the dependence of outlet temperatu-

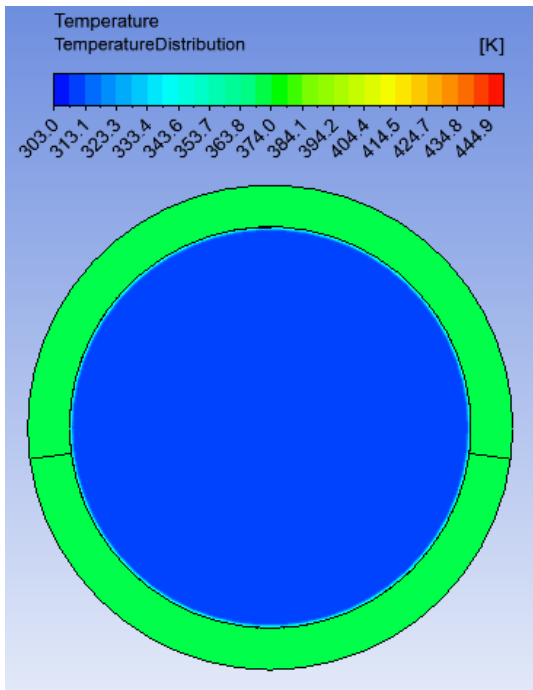


Figure 9: Temperature distribution at the absorber outlet for the reference immersed turbulizing device and fluid flow of $Q=0.25\text{dm}^3/\text{s}$

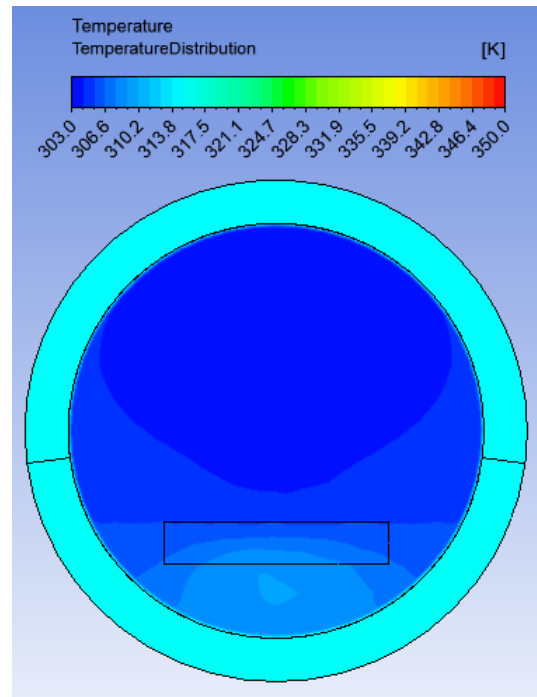


Figure 11: Temperature distribution at the absorber outlet for the vibrating plate and fluid flow of $Q=0.25\text{dm}^3/\text{s}$

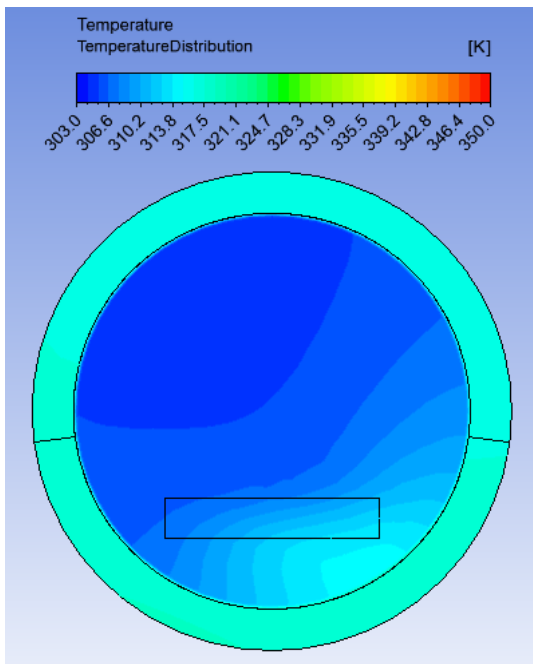


Figure 10: Temperature distribution at the absorber outlet for the vibrating plate and fluid flow of $Q=0.05\text{dm}^3/\text{s}$

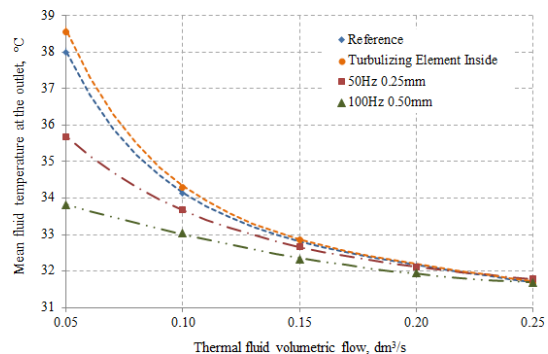


Figure 12: Mean temperature of the thermal fluid at the absorber outlet for respective modelled cases of absorber operation

The data shown in Fig. 12 shows that utilization of the vibrating plate was followed by a large drop in the mean temperature of the thermal fluid, whereas the immersed spiral turbulizing device led to an increase in the outlet temperature of approximately 0.6°C . Furthermore, the change in temperature is accentuated with low fluid flows, while for flows exceeding $0.15\text{dm}^3/\text{s}$ none of the simulated turbulization methods were followed by a change in fluid outlet temperature.

res and thermal efficiencies of respective absorbers are depicted in Fig. 12 and Fig. 13.

As regards the curves plotted in Fig. 13, the highest thermal efficiency for low flows was achieved for

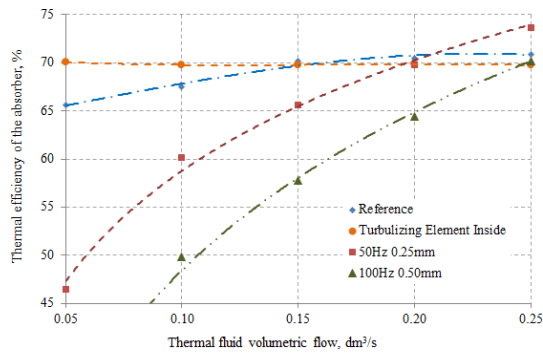


Figure 13: Mean thermal efficiency of the absorber, regarding total sunlight on the concentrating area, for respective modelled cases of absorber operation

Table 2: Heat gained by the thermal fluid for respective modelled cases of absorber operation

Case description	Max heat gain, W
Reference, no turbulization	709.0
Vibrating plate, $f=50\text{Hz}$, $\delta=0.25\text{mm}$	736.9
Vibrating plate, $f=100\text{Hz}$, $\delta=0.50\text{mm}$	701.6
Static spiral immersed in the fluid	700.8

the plate vibrating at low frequency and low amplitude. The decrease in thermal efficiency for vibration of higher frequency and amplitude might be caused by a significant backflow, causing a drop in real volumetric flow of the thermal fluid through the absorber. For the reference cases of absorber with no turbulence intensification and vibrating plates, absorber efficiency rises as fluid flow increases. Regarding the immersed device, thermal efficiency of the absorber remained roughly constant at 70%, independently of local flow. However, the highest thermal efficiency, 71%, was achieved for the vibrating plate at the highest of the investigated fluid flows.

The maximum total power gains of the flowing thermal fluid for simulated cases of absorber geometry are indicated in Table 2.

Analysis of the acquired data suggests that application of the vibrating plate might be successfully introduced to increase maximum heat gains from a single absorber. Careful consideration has to be given to amplitude and frequency of vibrations. As presented in Fig. 13 and Table 2, a rise in both amplitude and frequency of oscillations led to a significant drop in power gain and efficiency of the absorber, caused by a rise in backflow vertices at the absorber outlet. The intensification of backflow throttled the real flow of thermal fluid through the absorber. As shown in Fig. 13 and discussed in reference [38], a drop in the streamflow of the circulating fluid, composed of pure thermal fluid, is followed by a significant decrease in effective power gain. Nevertheless, utilization of a static turbulizing

device introduces an exception to this observation - as depicted in Fig. 13: independently of the coaxial volumetric flow, the power acquired from the absorber equipped with the immersed turbulizing device stays almost constant. This might be caused by a reduction in axial flow in the area enclosed between walls of the spiral device.

Thus, with respect to the overall effects of the investigated methods, utilization of the immersed turbulizing device seems to be the most beneficial solution, especially considering the low flows of the circulating fluid. For flows exceeding $0.2 \text{ dm}^3/\text{s}$, all simulated cases (including the reference) achieve a similar outlet temperature of the fluid, whereas low-amplitude vibration delivers the highest efficiency.

Contour distributions have been plotted for the respective cases to aid detailed analysis of the wall heat transfer coefficient at the interface between the absorber and the thermal fluid. The distributions are shown in Fig. 14 through Fig. 16.

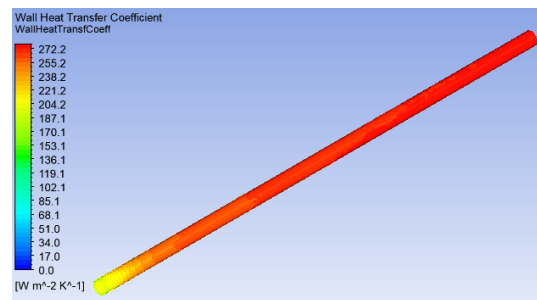


Figure 14: Local wall heat transfer coefficient values at the solid-liquid interface for the reference case with no flow turbulization

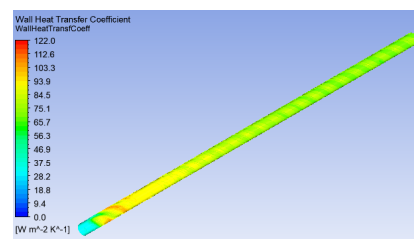


Figure 15: Local wall heat transfer coefficient values at the solid-liquid interface for the immersed turbulizing device case

In light of the results collected for the wall heat transfer analysis, distribution of local values of the coefficient is similar for both the reference case and the vibrating plate case, at the stable state of high thermal fluid flow.

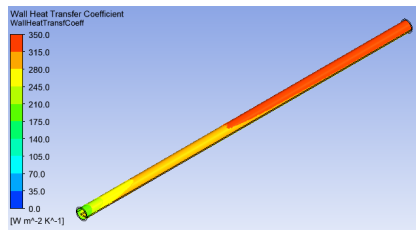


Figure 16: Local wall heat transfer coefficient values at the solid-liquid interface for the vibrating plate case

Nevertheless, for the two investigated geometries of the absorber, there are low coefficient values in the entrance region of the absorber, as shown in Fig. 14 and Fig. 16. Moving from the inlet towards the outlet along the concentric axis of the geometries, the values of the wall heat transfer coefficient rise almost linearly in both cases. This observation proves the insignificant effect of vibrations on heat transfer distribution on the outer interface of the thermal fluid domain.

However, considering the data acquired for the immersed turbulizing device, shown in Fig. 15, a significant change was observed in the distribution of the coefficient. In the middle of the volumes, constrained by the walls of the device, the wall heat transfer coefficient took higher values, although parts of the absorber were insulated by joint walls of the immersed device. Nonetheless, the highest values of the coefficient were observed at the initial turbulization of the flow, with a linear drop in the middle part of the absorber. This observation suggests that utilization of the turbulizing device might be especially valuable to enhance convection close to the inlet, but it is not necessarily beneficial for heat transfer intensification in the middle and end part of the absorber.

4 Conclusions

The results of the simulations indicate that vibrations at low acoustic frequencies have only a marginal impact in terms of enhancing heat transfer in the absorber of a vacuum solar collector. This is proven by no rise in thermal fluid outlet temperature being observed. Since fluid temperature could be a key parameter affecting the interconnection of the solar power system with other devices, the lack of a visible difference markedly limits the application of this method. One possible reason for this is the high viscosity of the phenyl-based thermal oil used as the working fluid for high temperature installations, which results in a thick, viscous boundary layer. As temperature distributions show, the simulated vibrations do not introduce sufficient kinetic energy to create significant

boundary layer vertices and turbulization of the fluid, which are required to enhance convection. Nevertheless, the results show that vibrations might be successfully applied to enhance the thermal efficiency of absorbers, especially for low fluid flows. Considering this parameter, the vibrating plate variant is the most favorable of all the simulated cases. Whereas for low feed flows the rise in thermal efficiency due to the vibrating plate may exceed 4%, the simulation did not factor in the significant rise in internal energy consumption required to induce vibrations or the additional costs of detailed analysis of the frequency and amplitude of oscillations. Therefore, there would be little real gain to be had from using this heat transfer intensification method.

The data collected for the immersed spiral turbulizing device prove its applicability in solar absorbers. The mean fluid temperature distribution at the absorber outlet, as well as the macroscopic thermal effects of absorber operation, prove the beneficial effect of introducing the immersed turbulizing element. However, the rise in operational parameters of the absorber is visible mostly for volumetric flows ($Q < 0.05 \text{ dm}^3/\text{s}$), which could limit application of this method. For intermediate and high fluid flows ($Q > 0.15 \text{ dm}^3/\text{s}$), the absorber equipped with the immersed device achieved efficiency comparable to the reference case, which was probably caused by pressure losses at the fluid-solid walls and a significant drop in mean fluid velocity inside the absorber. Nevertheless, optimization of the constructional features of the turbulizing element might solve these issues and broaden its applicability.

The results discussed in this paper concern the use of a medium which at ambient temperature is approximately 120 times more viscous than water [39]. The thick viscous boundary layer, which limited heat transfer in the simulated cases, might not correspond to the flow dynamics of other media, for example pressurized water. For such media, investigations covering a wide range of frequencies should be considered [35].

5 Acknowledgements

This scientific work was funded by the National Science Center within the framework of research project No. 2018/29/B/ST8/02406.

References

- [1] E. Klugmann and E. Klugmann-Radziemska. *Ogniwa i moduły fotowoltaiczne oraz inne niekonwencjonalne źródła energii*. Wydawnictwo Ekonomia i Środowisko, 2005.

- [2] G. Lobaccaro. A cross-country perspective on solar energy in urban planning: Lessons learned from international case studies. *Renewable and Sustainable Energy Reviews*, 108:209–237, 2019.
- [3] A. de la Calle, A. Bayon, and J. Pye. Techno-economic assessment of a high-efficiency, low-cost solar-thermal power system with sodium receiver, phase-change material storage, and supercritical CO₂ recompression Brayton cycle. *Solar Energy*, 199:885–900, 2020.
- [4] Q. Ye, M. Chen, and W. Cai. Numerically investigating a wide-angle polarization-independent ultra-broadband solar selective absorber for high-efficiency solar thermal energy conversion,. *Solar Energy*, 184:489–496, 2019.
- [5] M.S. Ryu, H.J. Cha, and J. Jang. Effects of thermal annealing of polymer: fullerene photovoltaic solar cells for high efficiency. *Current Applied Physics*, 10:s206–s209, 2010.
- [6] W. Gogół, O. Skonieczny, and L. Zakrzewski. *Niektóre zagadnienia wymiany ciepła w kolektorach energii promieniowania słonecznego*. Politechnika Warszawska, 1979.
- [7] M. Burhan, M. Wakil Shahzad, S. Jin Oh, and K. Choon Ng. Long Term Electrical Rating of Concentrated Photovoltaic (CPV) Systems in Singapore,. *Energy Procedia*, 158:73–78, 2019.
- [8] M. George, A.K. Pandey, N. Abd Rahim, V.V. Tyagi, S. Shahabuddin, and R. Saidur. Concentrated photovoltaic thermal systems: A component-by-component view on the developments in the design, heat transfer medium and applications. *Energy Conversion and Management*, 186:15–41, 2019.
- [9] N. Bushra and T. Hartmann. A review of state-of-the-art reflective two-stage solar concentrators: Technology categorization and research trends. *Renewable and Sustainable Energy Reviews*, 114:109307, 2019.
- [10] M. Sanchez, I.G. Martinez, E.A. Rincon, and M.D. Duran. Design and thermal-optic analysis of an ultra-solar concentrator,. *Energy Procedia*, 57:311–320, 2014.
- [11] M. El Ydrissi, H. Ghennioui H., E.G. Bennouna, and A. Farid. Geometric, optical and thermal analysis for solar parabolic trough concentrator efficiency improvement using the Photogrammetry technique under semi-arid climate. *Energy Procedia*, 157:1050–1060, 2019.
- [12] L. Evangelisti, R. De Lieto Vollaro, and F. Asdrubali. Latest advances on solar thermal collectors: A comprehensive review. *Renewable and Sustainable Energy Reviews*, 114:109318, 2019.
- [13] N.B. Desai, S. B. Kedare, and S. Bandyopadhyay. Optimization of design radiation for concentrating solar thermal power plants without storage. *Solar Energy*, 107:98–112, 2014.
- [14] M.A. Ehyaei, A. Ahmadi, M. El Haj Hassad, and T. Salameh. Optimization of parabolic through collector (PTC) with multi objective swarm optimization (MOPSO) and energy, exergy and economic analyses. *Journal of Cleaner Production*, 234:285–296, 2019.
- [15] J. Ruelas, D. Saucedo, J. Vargas, and R. García. Thermal and concentration performance for a wide range of available offset dish solar concentrators. *Applied Thermal Engineering*, 144:13–20, 2018.
- [16] G.H. Lee. Construction of conical solar concentrator with performance evaluation,. *Energy Procedia*, 153:137–142, 2018.
- [17] E.T.A. Gomes, N. Fraidenaich, O.C. Vilela, C.A.A. Oliveira, and J.M. Gordon. Aplanats and analytic modeling of their optical properties for linear solar concentrators with tubular receivers. *Solar Energy*, 191:697–706, 2019.
- [18] H. Mashaal, D. Feuermann, and J.M. Gordon. Expansive scope of aplanatic concentrators and collimators. *Applied Optics*, 58:F14–F20, 2019.
- [19] J.M. Gordon, D. Feuermann, and P. Young. Unfolded aplanats for high-concentration photovoltaics,. *Optical letters*, 33:1114–1116, 2008.
- [20] C. Michel. Waveguide solar concentrator design with spectrally separated light. *Solar Energy*, 157, 2017.
- [21] G. Wang, Y. Yao, Z. Chen, and P. Hu. Thermodynamic and optical analyses of a hybrid solar CPV/T system with high solar concentrating uniformity based on spectral beam splitting technology. *Energy*, 166:256–266, 2019.
- [22] J. Chen, L. Yang, Z. Zhang, J. Wei, and J. Yang. Optimization of a uniform solar concentrator with absorbers of different shapes. *Solar Energy*, 158:396–406, 2017.
- [23] K.A. Moharram, M.S. Abd-Elhady, H.A. Kandil, and H. El-Sherif. Model-based performance diagnostics of heavy-duty gas turbines using compressor map adaptation. *Enhancing the perfor-*

- mance of photovoltaic panels by water cooling, 4:869–877, 2013.
- [24] P. Selvakumar, P. Somasundaram, and P. Thangavel. Performance study on evacuated tube solar collector using Therminol D-12 as heat transfer fluid coupled with parabolic trough. *Energy Conversion and Management*, 85:505–510, 2014.
- [25] J. Qin, E. Hu, G.J. Nathan, and L. Chen. Simulating combined cycle gas turbine power plants in Aspen HYSYS. *Energy Conversion and Management*, 152:281–290, 2017.
- [26] M. Sabiha. An experimental study on Evacuated tube solar collector using nanofluids. In *International Conference on Advances in Science, Engineering, Technology and Natural Resources (ICASETNR-15) Sabah, Malaysia*, volume 2, pages 42–49.
- [27] H. Fathabadi. Novel solar collector: Evaluating the impact of nanoparticles added to the collector's working fluid, heat transfer fluid temperature and flow rate. *Renewable Energy*, 2019.
- [28] J. Spelling, A. Gillo, M. Romero, and J. Gonzalez-Aguilar. Simulation and analysis of humid air turbine cycle based on aeroderivative three-shaft gas turbine. *A High-efficiency Solar Thermal Power Plant using a Dense Particle Suspension as the Heat Transfer Fluid*, 69:1160–1170, 2019.
- [29] M.M. Heyhat, M. Valizade, Sh. Abdolhazade, and M. Maerefat. Thermal efficiency enhancement of direct absorption parabolic trough solar collector (DAPTSC) by using nanofluid and metal foam. *Energy*, 192:1166626, 2020.
- [30] A. García, R. Herrero-Martin, J.P. Solano, and J. Pérez-García. The role of insert devices on enhancing heat transfer in a flat-plate solar water collector. *Applied Thermal Engineering*, 132:479–489, 2018.
- [31] D. Jin, S. Quan, J. Zuo, and S. Xu. Numerical investigation of heat transfer enhancement in a solar air heater roughened by multiple V-shaped ribs. *Renewable Energy*, 33(2019):78–88, 2018.
- [32] F.A.S. da Silva, D.J. Dezan, A.V. Pantaleão, and L.O. Salviano. Longitudinal vortex generator applied to heat transfer enhancement of a flat plate solar water heater. *Applied Thermal Engineering*, 158:113790, 2019.
- [33] M.A. Sharafeldin, G. Gróf, E. Abu-Nada, and O. Mahian. Evacuated tube solar collector performance using copper nanofluid: Energy and environmental analysis. *Applied Thermal Engineering*, 162:114205, 2019.
- [34] W. Liu, Z. Yang, B. Zhang, and P. Ly. Experimental study on the effects of mechanical vibration on the heat transfer characteristics of tubular laminar flow. *International Journal of Heat and Mass Transfer*, 115 (Part A):169–179, 2017.
- [35] M. Setareh, M. Saffar-Avval, and A. Abdullah. Experimental and numerical study on heat transfer enhancement using ultrasonic vibration in a double-pipe heat exchanger. *Applied Thermal Engineering*, 159:113867, 2019.
- [36] L. Cheng, T. Luan, W. Du, and M. Xu. Heat transfer enhancement by flow-induced vibration in heat exchangers. *International Journal of Heat and Mass Transfer*, 52:1053–1057, 2009.
- [37] A. Hosseinian and A.H. Meghdadi Isfahani. Experimental study of heat transfer enhancement due to the surface vibrations in a flexible double pipe heat exchanger. *Heat and Mass Transfer*, 54:1113–1120, 2018.
- [38] K. Grzywnowicz, Ł. Bartela, L. Remiorz, and B. Stanek. Modeling of influence of vibration on intensification of heat transfer within the absorber of the vacuum solar collector. In *XIV Research and Development in Power Engineering Conference*, volume 137, page 01034. E3S Web of Conferences, 2019.
- [39] Solutia-Europe. *Therminol® VP-1 High Performance Highly Stable Heat Transfer Fluid*, 2016.
- [40] C.G. Speziale, S. Sarkar, and T.B. Gatski. Modeling the Pressure-Strain Correlation of Turbulence: an Invariant Dynamical Systems Approach. *Journal of Fluid Mechanics*, 227:245–272, 1991.
- [41] ANSYS. *ANSYS CFX-Solver Theory Guide. Release 15.0*, 2013.
- [42] K. Wood, B. Whitney, J. Bjorkman, and M. Wolff. *Introduction to Monte Carlo Radiation Transfer*. The Astronomy Group of University of St Andrews, 2013.